Plasma Chem Plasma Process (2017) 37:1505–1522
DOI 10.1007/s11090-017-9837-3

ORIGINAL PAPER

Transport Coefficients of Two-temperature Lithium Plasma for Space Propulsion Applications

Guangqing Xia[1] · Yajie Han[1] · Qiuyun Wu[1] · Liuwei Chen[1] · Niandong Zhou[1]

Received: 11 May 2017 / Accepted: 29 July 2017 / Published online: 30 August 2017

Abstract Lithium has been proposed as an attractive metal propellant for advanced electric propulsion. In our current work, transport coefficients including the viscosity, thermal conductivity, and electrical conductivity of lithium plasma under both the equilibrium and non-equilibrium conditions are calculated based on a two-temperature model. The collision integrals used in calculating the transport coefficients are significantly more accurate than values used in previous theoretical studies, resulting in more reliable values of the transport coefficients. Results are computed for different degrees of thermal non-equilibrium, i.e. the ratio of electron to heavy particle temperatures, from 1 to 15, with the electron temperature ranging from 300 to 60,000 K in a wide pressure range from 0.0001 to 100 atm. We compare our calculated results with existing published results and discrepancies are found and explained.

Keywords Lithium · Non-equilibrium plasma · Two-temperature model · Collision integral · Transport coefficients · Chapman–Enskog method

Introduction

Lithium is a favorite propellant in Magnetoplasmadynamic Thruster (MPDT) and has several advantages over more conventional propellants [1, 2]. Firstly, Lithium has a lower first ionization potential (5.4 eV) and a higher second ionization potential (75.6 eV) compared to other propellants. This special feature can reduce the ionization loss and the frozen flow loss in the thruster, leading to a higher thrust efficiency. Moreover, Lithium can reduce the work function of tungsten (the material from which the cathode is made) from 4.5 to 2.1 eV when barium is used as an additive, decreasing erosion and increasing the

✉ Guangqing Xia
gq.xia@dlut.edu.cn

[1] State Key Laboratory of Structural Analysis for Industrial Equipment, School of Aeronautics and Astronautics, Dalian University of Technology, Dalian 116024, China

lifetime of the thruster. The numerical simulation of MPDT or other types of electric propulsion thrusters is very useful in providing more insight into the improvement of their operation performance. For this, a Magnetohydrodynamics (MHD) model, which usually involves the solution of the mass, momentum and energy equations of the working plasma medium and the solution of the electromagnetic field equations strongly coupled with the plasma dynamical equations, had been developed and is widely used [3, 4]. To obtain the thermodynamic and transport properties of the working medium (plasma) appearing in the governing equations are a prerequisite of the solution of a MHD model and thus needed to be known in advance. The most reliable way to obtain these properties is the kinetic theory of ideal gases for thermodynamic properties and the approximate solution of the Boltzmann equation based on the Chapman–Enskog method for transport coefficients [5]. For the case of plasmas in local thermodynamic equilibrium (LTE) which is often assumed in the MHD model, calculated results of the thermodynamic properties and transport coefficients of many types of thermal plasmas are available [6–21].

When large temperature gradient (existing near a cold wall or when cold vapor is injected in the plasma) or insufficient electron number density to achieve efficient energy exchange between electrons and heavy particles, the assumption of local thermodynamic equilibrium (LTE) is no longer valid [22]. Under such circumstances, when the conditions for local chemical equilibrium are fulfilled, the electrons and heavy particles are able to maintain their Maxwellian velocity distribution functions separately but have different temperature. A two-temperature MHD model would thus be required to describe the non-equilibrium plasma behavior, in which the electrons and heavy particles follow different energy conservation equations [23–30]. For the computation of non-equilibrium (NLTE) thermodynamic and transport properties, two theories have been developed: Devoto [31] and Bonnefoi [32] developed a simplified theory which considers complete decoupling between heavy particles and electrons and Rat et al. [33] developed a theory in which the coupling between particles and electrons is fully taken into account. Recently, Zhang et al. [34, 35] derived new expression of transport coefficients for two temperature plasma by adopting reasonable simplifications based on the physical fact that the masses of electrons are much smaller than those of heavy species. This can greatly save the calculation time of transport coefficients by Rat et al.'s method. Meanwhile, the coupling between electrons and heavy species is taken into account leading to more accurate expressions of transport coefficients than those by complete decoupling between heavy particles and electrons. Transport properties of two-temperature plasma have already been calculated for a wide range of pure gases and mixtures in the literature [36–50]. A recent study [49, 50] of non-LTE transport properties based on a comparison of the approaches of Devoto and Rat et al. shows that coupling between electrons and heavy particles does not lead to significant changes in the predicted non-equilibrium plasma transport properties, except for certain ordinary diffusion coefficients. No significant discrepancies occur in the thermal conductivity, viscosity or electrical conductivity, even when they depend on the ordinary diffusion coefficients.

In this work, results for equilibrium and non-equilibrium transport properties of lithium plasma are presented by using a two-temperature plasma model. To our knowledge, thermodynamic properties and transport coefficients of two-temperature lithium plasma have been published in the literature for the pressure range from 0.0001 to 1 atm, electron temperatures from 1000 to 40,000 K and the electron/heavy particle ratio from 1 to 5 [51]. These data are useful for fluid dynamic simulation of most MPD thrusters but they are not enough in some extreme operating conditions where the temperature and pressure may exceed 40,000 K and 1 atm respectively. Also, near the wall, the non-equilibrium

parameter can reach values beyond 5. Additionally, more accurate representations of the intermolecular potentials, which can reduce the uncertainties in the values of transport coefficients, are available in the literature. Therefore, in our current work, transport properties results calculated by using the cross-section data with highest accuracy are presented and discussed over a wider electron temperature range of 300–60,000 K, pressure range from 0.0001 to 100 atm and electron/heavy particle ratio from 1 to 15. We also compared our results with the published data and the possible reasons for the discrepancies analyzed. Note that lithium propellant exists in the form of condensed phase in the temperature range lower than its boiling point of 1603 K. The reason for considering temperatures lower than 1603 K in our current work is to achieve convergence in numerical simulations. It has been observed that even though the minimum temperature in a final converged solution may not be lower than 1603 K, it may easily exceed this limit at some intermediate stages of the computation. Unavailability of property data, physically compatible with the associated temperature variation, often leads to divergence of the simulation.

Calculation of Two-Temperature Plasma Composition

Transport properties under both the equilibrium and non-equilibrium conditions depend strongly on the species composition. The plasma composition under the LTE condition can be calculated by either the mass action law (Saha and Guldberg–Waage laws) with the Dalton and species conservation laws as the neutral condition or the Gibbs free energy minimization method [52], whereas the appropriate method for the determination of chemical equilibrium number densities in two-temperature plasmas has long been a subject of debate because different formulas for ionization and dissociation equilibrium are obtained when different thermodynamic constraints are imposed [22, 53–62] and there exist two typical forms of the mass action law, represented by Potapov's method [53] and Van de Sanden et al.'s method [54]. Wang et al.'s work for two-temperature SF_6 plasma finds that the difference in the forms of the mass action law leads to significant discrepancy in species composition and hence the plasma properties [63]. For example, Potapov's approach leads to larger variation in species concentration and plasma properties at high non-equilibrium degree, especially the properties to which the chemical reaction contributes apparently. In this work, we have used the method proposed by van de Sanden et al. [54] due to the fact that Van de Sanden's approach has been widely cited in literature as a reference case for chemical equilibrium calculations.

The plasma of a two-temperature lithium plasma system consists of five components, i.e. lithium atoms Li, singly-ionized ions Li^+, doubly-ionized ion Li^{2+}, triply-ionized ion Li^{3+} and electrons e^-. We include triply-ionized ion Li^{3+} because its molar fraction can reach 1% at the highest temperature around 60,000 K under the lowest pressure of 0.0001 atm. A total of 3 independent reactions, i.e. the continuous ionization of Li $Li^{r+} \leftrightarrow Li^{(r+1)+} + e^-$, are taken into account and described by the mass action law, i.e. Saha's equation for ionization reactions, which are described as follows.

$$n_e\left[\frac{n_{\mathrm{Li}^{(r+1)+}}}{n_{\mathrm{Li}^{r+}}}\right] = 2\left[\frac{Q_{\mathrm{Li}^{(r+1)+}}(T_e)}{Q_{\mathrm{Li}^{r+}}(T_e)}\right]\left[\frac{2m_e\pi kT_e}{h^2}\right]^{3/2}\exp\left[-\frac{E_{I,r+1}-\delta E_{I,r+1}}{kT_{ex}}\right] \quad (1)$$

where Q is the internal partition function with subscript r represents r-times ionized species. $E_{\mathrm{I},r+1}$ is the ionization energy; k and h are the Boltzmann constant and Planck

constant. n_i and m_i are the number density and mass of specie i. T_{ex} is the excitation temperature of species Li^{r+} ionization which is characterized by the electron temperature T_e. $\delta E_{I,r+1}$ is the lowering of the ionization energy. The species partition functions are then computed following the suggestion of Wang et al. [46]. Data of the electron energy levels of atoms and ions for the evaluation of their partition functions and the ionization energies have been taken from the NIST database [64]. To be concrete, their values are 5.4, 75.6 and 122.5 eV, respectively, for the lithium plasma.

In addition to the law of mass action (Saha's law) as detailed above, the equations governed by the Dalton's Law for equation of state, and electrical quasi-neutrality are required which are described as follows.

$$P = n_e k T_e + \sum_i n_i k T_h \tag{2}$$

$$\sum_i n_i Z_i = 0 \tag{3}$$

where T_h is the heavy particle temperature, P and Z_i are the pressure and the charge of species i.

Chemical equilibrium compositions as a function of electron temperature for different values of the non-equilibrium parameter $\theta = T_e/T_h$ are shown in Fig. 1. At $P = 1$ atm, the ionization of lithium atoms occurs at a relative low electron temperature around 4000 K because of a comparatively lower ionization potential 5.4 eV. The species molar fractions keep almost constant in a wide temperature range from 10,000 to 45,000 K because the second ionization potential is extremely high (eV) and no further ionization takes place in the plasma system. At around 50,000 K, the electrons energy is high enough to ionize the singly-ionized ions Li^+ into Li^{2+}. As a result, the molar fraction of doubly-ionized ion Li^{2+} gradually rises. Only the monoatomic species are taken into account in the lithium plasma and the ionization reaction is dominantly controlled by the excitation temperature,

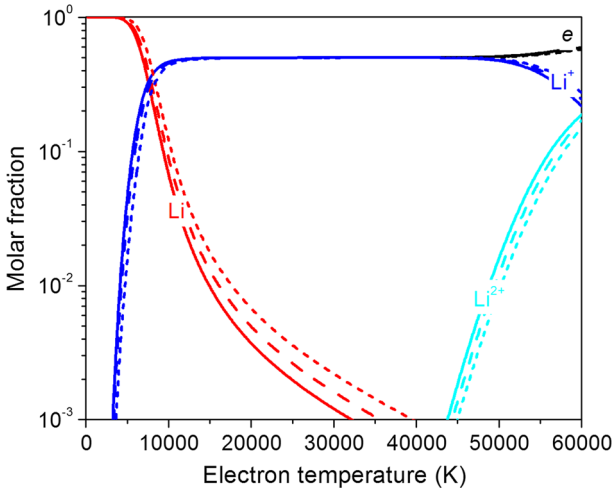

Fig. 1 Electron temperature dependence of the mole fractions of different species at $P = 1$ atm for different values of the non-equilibrium parameter: *Solid line*: $\theta = 1$; *dashed line*: $\theta = 2$; *short dashed line*: $\theta = 10$

i.e. the electron temperature. Therefore, the influence of the non-equilibrium parameter on the calculated species molar fraction is minor at a fixed electron temperature. We can observe the electrons mole fraction decreases with growing value of θ, though electron number density increases (not shown). As mentioned above, the extremely low first-ionization potential and high second-ionization potential benefits the thrust generation and reduces the flow frozen flow loss.

The influence of different pressures on the chemical equilibrium compositions of two-temperature lithium plasma is presented in Fig. 2. The increase of gas pressures prohibits the ionization reactions and leads to a lower ionization degree and hence decreased molar fractions of charged species at a fixed electron temperature. Following the work of Wang et al. [46], this trend can be explained according to Le Chatelier's law: the increase of the pressure opposes changes to the original state of equilibrium, so that chemical reactions at a given temperature are suppressed.

Collision Integrals

The expressions for the transport coefficients depend on the collision integrals, which are averages over a Maxwellian distribution of the transport cross sections for the binary interactions between species and defined as follows [5]:

$$\Omega_{ij}^{(l,s)} = \sqrt{\frac{kT_{ij}^{*}}{2\pi\mu_{ij}}} \int_{0}^{\infty} \exp\left(-\gamma_{ij}^{2}\right) \gamma_{ij}^{2s+3} Q_{ij}^{l}(g) d\gamma_{ij} \tag{4}$$

Here γ_{ij} is the reduced initial speed of the colliding molecules i and j, given by

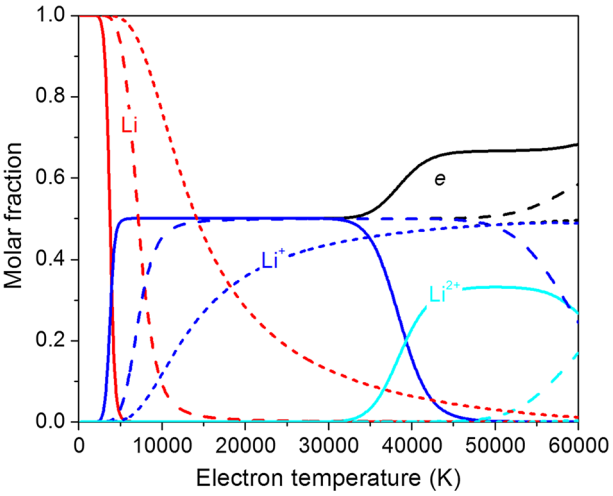

Fig. 2 Electron temperature dependence of the mole fractions of different species at the non-equilibrium parameter of $\theta = 2$ for different values of pressures. *Solid line*: 0.0001 atm; *dashed line*: 1 atm; *short dashed line*: 10 tam

$$\gamma_{ij} = \sqrt{\frac{\mu_{ij}}{2kT_{ij}^*}} g_{ij} \tag{5}$$

where g_{ij} is the initial relative speed of the colliding molecules i and j. T_{ij}^* and μ_{ij} are the reduced mass and the effective temperature of collision defined as [36]

$$\frac{1}{\mu_{ij}} = \frac{1}{m_i} + \frac{1}{m_j} \tag{6}$$

$$T_{ij}^* = \frac{(m_i T_j + m_{jT_i})}{m_i + m_j} \tag{7}$$

The transport cross sections [see Eq. (4)] are defined by

$$Q_{ij}^l(g) = 2\pi \int_0^\infty (1 - \cos^l \chi) b db \tag{8}$$

where b and r_m are the impact parameter and the outermost root of the Eq. (9) and $\varphi_{ij}(r)$ is the potential energy of interaction between the colliding particles. χ is the angle of deflection given by the expression (10).

$$1 - \frac{\varphi_{ij}(r)}{\frac{1}{2}\mu_{ij} g_{ij}^2} - \frac{b^2}{r_m^2} = 0 \tag{9}$$

$$\chi = \pi - 2b \int_{r_m}^\infty \frac{dr/r^2}{\sqrt{1 - \left[\varphi_{ij}(r) \Big/ \frac{1}{2}\mu_{ij} g_{ij}^2\right] - (b^2/r^2)}} \tag{10}$$

Computation of transport properties up to the third order requires the knowledge of collision integrals. $\Omega_{ij}^{(l,s)}$ with l and s satisfying the following conditions: $1 \leq l \leq 3$, $l \leq s \leq 5$.

For interactions in which charge exchange occurs collision integrals with odd value of l, including both elastic and inelastic processes, can be estimated by an empirical mixing rule [6]:

$$\Omega^{(l,s)} = \sqrt{\left(\Omega_{in}^{(l,s)}\right)^2 + \left(\Omega_{el}^{(l,s)}\right)^2} \tag{11}$$

where the subscripts in and el denote the collision integrals derived from the inelastic and the elastic interactions, respectively.

Collision integrals with even values of l are wholly determined by the elastic interactions [6].

$$Q_{ex} = (A - B \ln E)^2 \tag{12}$$

where E is the kinetic energy of the colliding particles. The constants A and B can be obtained from experimental data or theoretical calculations.

These transport cross sections for electron-neutral species interactions are obtained by numerically integrating the differential cross sections $d\sigma/d\Omega$ over all scattering angles as a function of the interaction energy as follows [47].

$$Q^{l}(E) = 2\pi \int_{0}^{\pi} \frac{d\sigma}{d\Omega} \sin\theta (1 - \cos\theta^{l}) d\theta \tag{13}$$

where E is the total kinetic energy of the colliding particles, dominated by the electron energy. Differential cross sections $d\sigma/d\Omega$ are determined by either experiment or through theoretical computation.

For Li–Li interactions, the collision integral is the statistical average of the collision integral for lowest singlet $X^1\Sigma_g^+$ Li_2 [65] and triplet state $X^3\Sigma_u^-$ Li_2 [66] interaction potentials which are based on the a priori potential and ab initio calculations respectively and accurately fitted by the Hulburt–Hirschfelder (H–H) potential. The fitted parameters are $\alpha = 2.362$, $\beta = 3.669$, $\gamma = 1.406$, $r_e = 2.696$ Å, $D_e = 1.033$ eV for $X^1\Sigma_g^+$ Li_2 and $\alpha = 3.530$, $\beta = 1.338$, $\gamma = 3.500$, $r_e = 4.452$ Å, $D_e = 0.0304$ eV for $X^3\Sigma_u^-$ Li_2.

For Li–Li^+ interactions, the elastic collision integral is determined by fitting the lowest two states to the exponential repulsive potential ($V_0 = 18.207$ eV, $\alpha = 0.754$ $Å^{-1}$) and the Hulburt–Hirschfelder (H–H) potential ($\alpha = 2.072$, $\beta = -1.702$, $\gamma = 2.342$, $r_e = 2.980$ Å, $D_e = 1.278$ eV) for the repulsive ($^2\Sigma_g^+$) and attractive states ($^2\Sigma_u^+$), respectively [67]. The charge-exchange cross-section for collisions between Li and Li^+ is determined by fitting Eq. (12) to the experimental results by Lorents et al. [68]. The constants A and B for the approximation of charge exchange cross sections are 19.3 and 3.5 Å respectively. Note that the determination of charge transfer collision integrals needs the cross sections data as a function of incident ion energy from zero to an enough high value. However, no available absolute cross section for charge transfer between lithium ions and lithium atoms below 14 eV were experimentally obtained by Lorents et al. [68] and other literature. Moreover, the theoretical calculations of Li–Li^+ charge transfer cross section always lead to some large underestimation when compared with the experimental values [69]. Indeed, the fact that the experimental curve lies somewhat higher than the theoretical one is also true for Caesium [68]. Considering the fact that the shapes of both the theoretical and experimental curves can be well represented by the formula (12), we have decided to use the transport cross section by choosing a best fit to beam measurements by Lorents et al. [68] and extrapolated it to a low-energy situation. Collision integrals with even values of l are wholly determined by the elastic interactions.

The elastic collision integrals for interactions between Li and doubly-ionized ion Li^{2+}, triply-ionized ion Li^{3+} are derived using a polarization potential. A value of Li polarizability 164.0 $Å^3$ [70] is used. The charge-exchange cross-section is small compared to the elastic collision cross-sections and is neglected in this paper.

In the case of electron collision with lithium atom, the elastic momentum-transfer cross section obtained theoretically by using the convergent close-coupling approach is available in literature [71] and the differential elastic scattering cross-sections from [72] are used to obtain the ratio $Q_2(E)/Q_1(E)$ and $Q_3(E)/Q_1(E)$ by straightforward integration.

Finally, the collision integrals for the charged–charged interactions were calculated using the screened Coulomb potential screened at the Debye length by the presence of charged particles. The effective collision integrals were calculated from the works of Mason et al. [73, 74], where the Debye length is calculated taking into account both the electrons and ions. Note that different choices of an appropriate form of shielding distance

in the estimation of collision integrals under screened coulomb potential can bring some deviation of calculated transport coefficients when ionization takes place. The influence of the choice of Debye length definition on the transport coefficients for two-temperature non-equilibrium plasma was investigated in the literature [47, 75] and is beyond our current scope.

Determination of Two-Temperature Transport Coefficients

The computation of transport properties is completed using the classical Chapman–Enskog method [4, 76, 77], assuming that the distribution functions of particles are first order perturbations to the Maxwellian distribution; perturbations are then expressed in series of Sonine polynomials, finally leading to a system of linear equations that can be suitably solved to obtain different transport properties. The simplified approach of Devoto [30] and Bonnefoi [32] which fully decouples the electrons and heavy particles is used in the present work because the coupling between electrons and heavy particles has no relevant effects on the prediction of non-equilibrium plasma transport properties presented in our work. For this, it is assumed that change in the perturbation function in electrons is greater than that of heavy particles in interactions involving both types of particles. Transport properties are calculated using the third-order approximation except for viscosity for which the second-order approximation has been adopted and can ensure enough high calculation accuracy.

Of the transport coefficients in two-temperature plasma, the reactive thermal conductivity is associated with the energy transport contributed by chemical reactions which absorb or release energy, leading to additional heat flux. The reactive thermal conductivity components of electrons and heavy particles are separately determined by an expression derived through reactive heat flux treating electrons and heavy particles separately [36, 78].

$$\lambda_{re} = \left[\sum_{r=1}^{v} \Delta h_r \frac{n}{\rho k T_h} \sum_{j=1}^{w} \frac{T_h}{T_j} m_j D_{rj}^{a} \frac{\partial p_j}{\partial T_e} \right]$$

$$\lambda_{rh} = \left[\sum_{r=1}^{v} \Delta h_r \frac{n}{\rho k T_h} \sum_{j=1}^{w} \frac{T_h}{T_j} m_j D_{rj}^{a} \frac{\partial p_j}{\partial T_h} \right] \tag{14}$$

where n, v and Δh_r are, respectively, total number density of all species, number of chemical reactions and reaction enthalpy change of reaction r. P_j is the partial pressure of specie j. D_{rj}^{a} is the ambipolar diffusion coefficient defined in terms of ordinary diffusion coefficients [36] which is a prerequisite to (14) and is determined following the framework of Hirschfelder et al. [4]. The partial derivative of partial pressure with respect to T_h and T_e $\partial p_j/\partial T_e$ and $\partial p_j/\partial T_h$ is determined by differentiating the partial pressure equation (from Dalton's law) with respect to T_h and T_e which are treated as independent variables. When the thermal conductivity is evaluated in terms of heavy particle temperature gradient, a total reactive thermal conductivity can be defined as [79].

$$\lambda_{reac} = \lambda_{re}\theta + \lambda_{rh} \tag{15}$$

The presence of an internal degree of energy freedom affects the heat flux vector and gives rise to an internal thermal conductivity component λ_{in}. It is derived using the Hirschfelder–Eucken approximation [80].

The total thermal conductivities for electrons and heavy particles, designated as λ_e and λ_h, can be expressed, respectively, as

$$\lambda_e = \lambda_{tre} + \lambda_{re}$$

and

$$\lambda_h = \lambda_{trh} + \lambda_{rh} + \lambda_{in} \tag{16}$$

where λ_{tre} and λ_{trh} are the translational thermal conductivity components of electrons and heavy particles.

A total thermal conductivity including the contributions of electrons and heavy particles are defined as follows:

$$\lambda_{tot} = \lambda_{trh} + \lambda_{tre} + \lambda_{reac} + \lambda_{in} \tag{17}$$

Two-temperature transport coefficients, namely electrical conductivity, Viscosity and thermal conductivity, are calculated at atmospheric pressure for different values of the non-equilibrium parameter $\theta = T_e/T_h$. The calculations are focused on $\theta = 1$, 2, 5, 10 and 15, whereas $\theta = 15$ is an extreme value which can be observed, at atmospheric pressure, as soon as the plasma interacts with a cold wall or when a injected cold gas or a low current is used [23–30].

Viscosity

Figure 3 presents variations of viscosity with electron temperature and non-equilibrium parameter. The viscosity of a gas increases till ionization starts at around 5,000 K due to the decrease of the collision integrals between neutral atoms. However, once ionization starts, long-range coulomb interaction increases with enhanced ionization and results in the observed drop in the viscosity value of two-temperature lithium plasma. We can also find that the peak locations show little dependence on the non-equilibrium parameters. This is

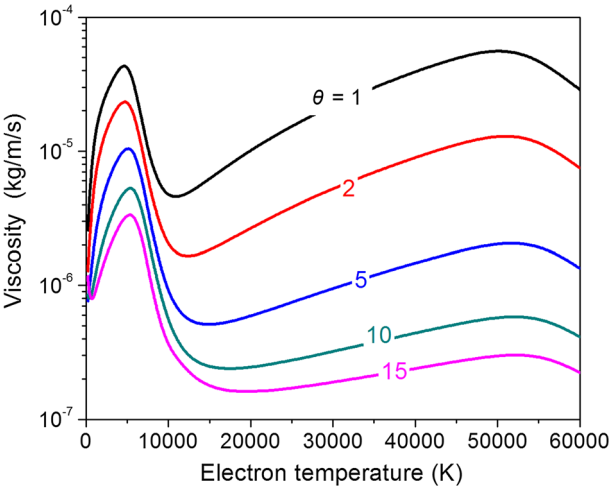

Fig. 3 Viscosity of two-temperature lithium plasma for different non-equilibrium parameters at atmospheric pressure

because the ionisation is mainly controlled by the electron temperature as mentioned above. Above 10,000 K, the viscosity increases because of the decreasing collision integrals for the charged–charged interactions with the temperature until a second peak which corresponds to the second ionisation is reached at around 50,000 K. Above 50,000 K, the occurrence of doubly ionised ions leads to a higher coulomb interaction and hence a drop of viscosity. For a given electron temperature, if non-equilibrium parameter increases, the heavy particle temperature decreases, resulting in a drop in the momentum transport and hence a drop in the viscosity value. With increasing θ, the peaks in the viscosity slightly shift towards higher electron temperature values.

Electrical Conductivity

The electrical conductivity is a property of electrons alone and depends only on collision integrals for interactions involving electrons. Its variation with electron temperature for different non-equilibrium parameters at atmospheric pressure is presented in Fig. 4. At a fixed electron temperature, higher non-equilibrium parameter values leads to higher electrical conductivities because of the increasing electron number density.

Thermal Conductivity

Various components of the total thermal conductivity (see formula 17) of two-temperature lithium plasma under the non-equilibrium condition are presented in Fig. 5. In the range of temperature where ionization take place, a great contribution to total thermal conductivity is given by the reactive term at around 7500 K whereas for high temperature the translational contribution from the electrons is the most important; internal thermal conductivity gives always a scarce contribution to total conductivity. The translational contribution from heavy particle dominates in the low temperature range when the ionization does not take place.

The variation of the total thermal conductivity for heavy particles and electrons (λ_h, λ_e) is shown in Figs. 6 and 7, respectively. The first and second peak of heavy particle thermal

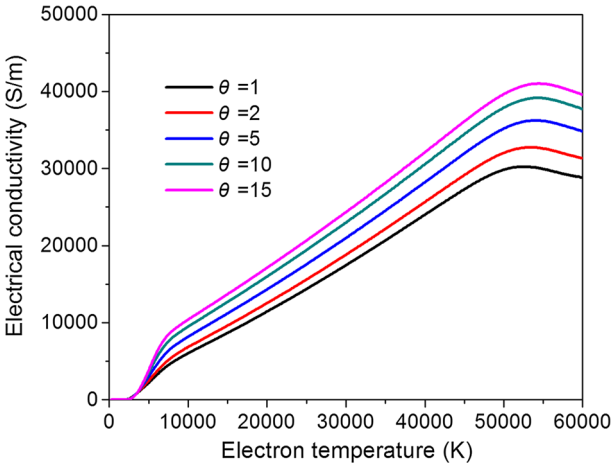

Fig. 4 Electrical conductivity of two-temperature lithium plasma for different non-equilibrium parameters at atmospheric pressure

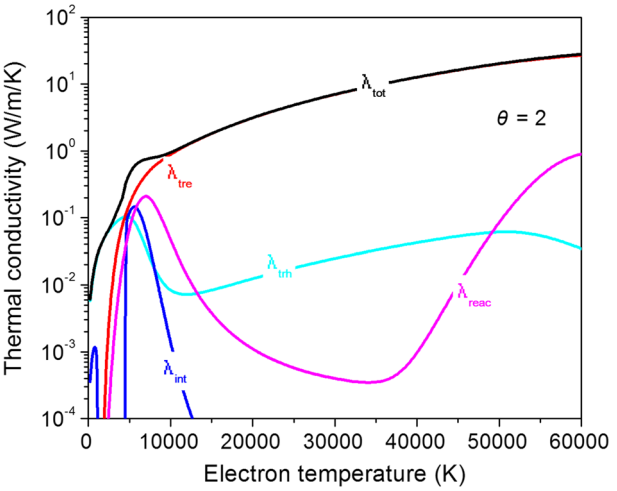

Fig. 5 Different thermal conductivity components of two-temperature lithium plasma with a non-equilibrium parameter of 2 at atmospheric pressure. λ_{tot} total thermal conductivity, λ_{trh} and λ_{tre} translational components due to heavy particles and electrons respectively, λ_{re} reactive component, λ_{in} internal component

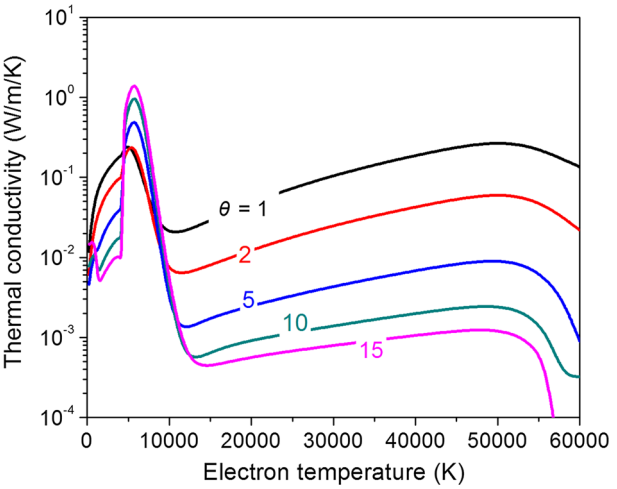

Fig. 6 Heavy particles thermal conductivity (λ_h) of two-temperature lithium plasma with different non-equilibrium parameters at atmospheric pressure

conductivity in Fig. 6 corresponds to the first and second ionization of lithium. The peak of the total thermal conductivity for electrons, which is linked with the ionization reaction, is not apparent because the translational component increases fast than the reaction component upon increasing electron temperature. In the temperature range below 5000 K and above 7500 K, the total thermal conductivity for heavy particles decreases with higher non-equilibrium parameters at a fixed electron temperature. This is because the heavy particle temperature decreases and hence the collision integrals between heavy particles rises. Electron thermal conductivity shows a slight increment as non-equilibrium parameter

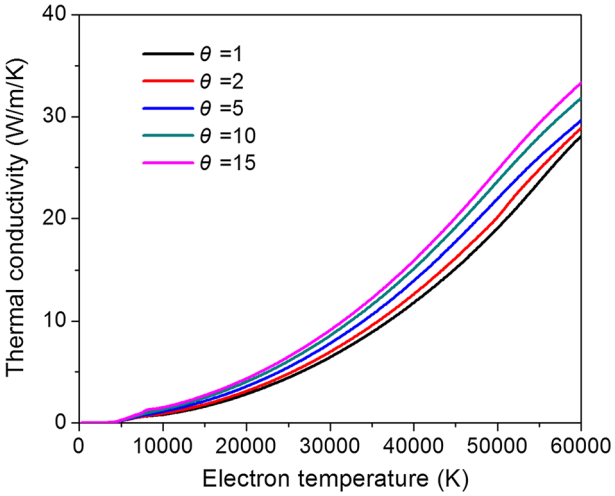

Fig. 7 Electrons thermal conductivity (λ_e) of two-temperature lithium plasma with different non-equilibrium parameters at atmospheric pressure

increases for fixed electron temperature, since the translation component which dominates in the high temperature range is a property which depends mainly on electrons.

Influence of Different Pressures on the Calculated Transport Coefficients

The influence of different pressures on the calculated transport coefficients is described in Fig. 8. In the temperature range where ionisation does not take place, the pressures show no apparent influence on the calculated viscosity, thermal conductivity and electrical conductivity of two-temperature lithium plasma. When the ionization occurs, as mentioned above in "Calculation of two-temperature plasma composition"section, the increasing pressures shift the ionisation to a higher electron temperature. This can explain the viscosity peak related to the first and second ionisation occurring at a higher electron temperature when the pressure rises. Similar mechanism can explain the fact the peak value of electrical conductivity which occurs for the lower pressure of 0.0001, 0.01 and 1 atm does take place in the temperature range considered here for the higher pressures of 10 and 100 atm. Moreover, it is noted that the viscosity, thermal conductivity and electrical conductivity increases with increasing pressure. For viscosity, a higher maximum value is because of the suppression of ionization, which means that the strong Coulomb interactions do not dominate until higher temperatures. For electrical conductivity, their higher values with a higher pressure are attributed to the fact that a higher pressure leads to a higher electron number density at a fixed electron temperature. For thermal conductivity, a higher electron number density brings a higher electron translational thermal conductivity and hence higher total thermal conductivity.

Comparison with Existing Data

The comparison of our calculated transport coefficient with previously published results under the local thermodynamic equilibrium condition is presented in Fig. 9. Although a different source of collision interaction is used here, our calculated viscosity and thermal

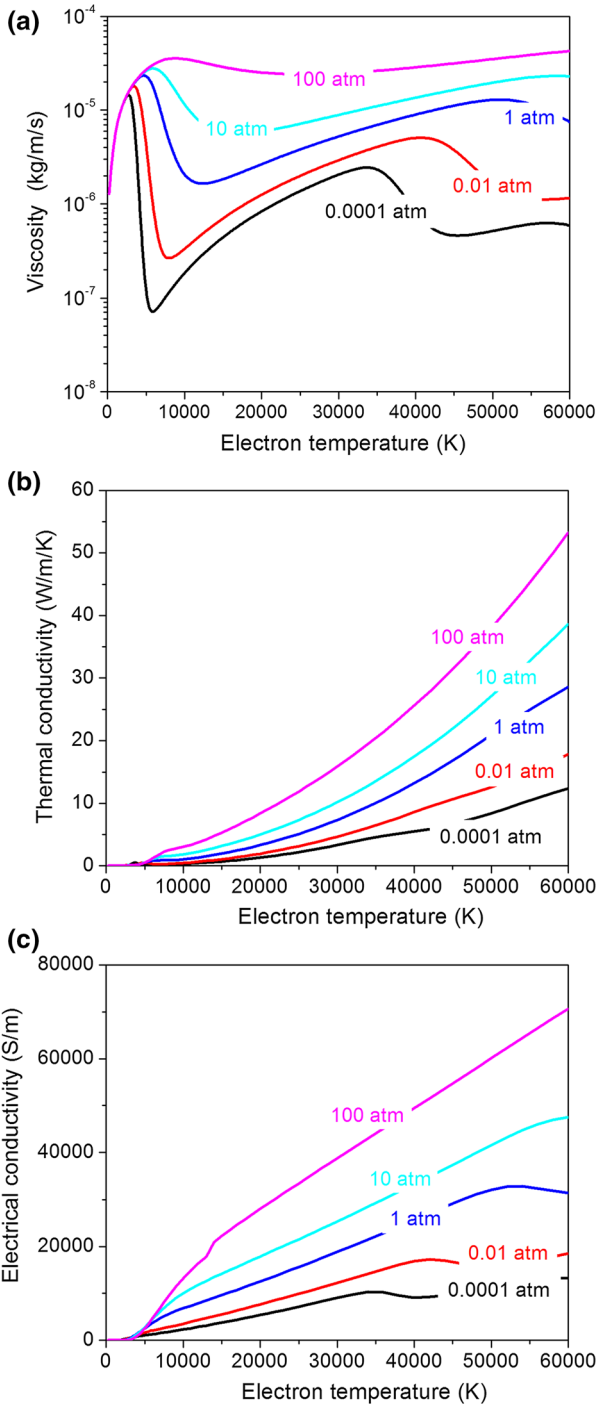

Fig. 8 Calculated viscosity, thermal conductivity and electrical conductivity of two-temperature lithium plasma with a non-equilibrium parameter of $\theta = 2$ under different pressures

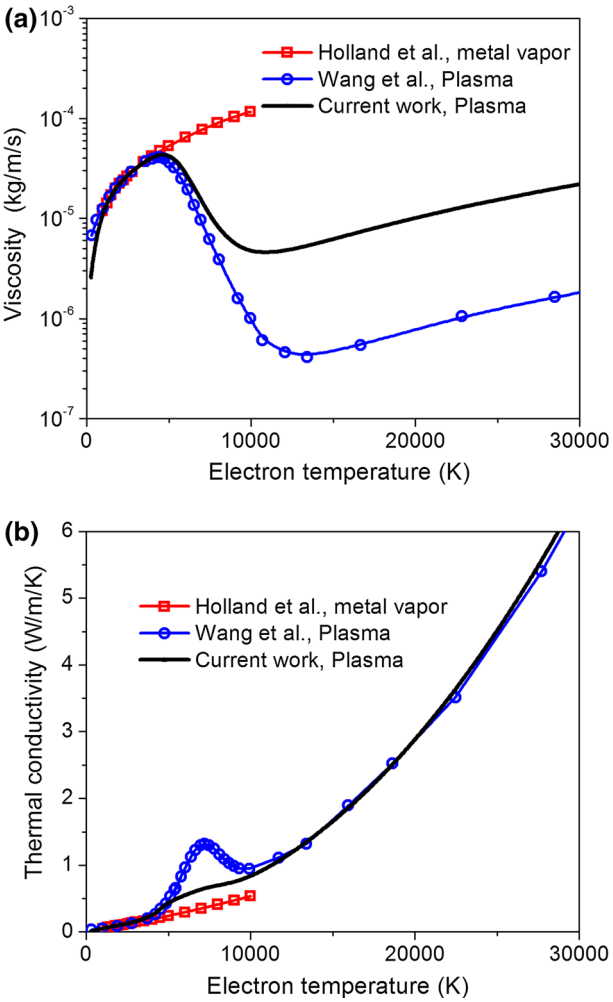

Fig. 9 Comparison of the equilibrium transport coefficients of lithium plasma from the present work with those of Holland et al. [81] and Wang et al. [51] at atmospheric pressure **a** viscosity and **b** total thermal conductivity

conductivity show good agreement with the results calculated by Gleizes et al. [82] and Wang et al. [42] in the low temperature range below around 4000 K where the interaction between lithium atoms dominates. Both Gleizes et al. [82] and Wang et al. [42] used the same collision integral values for Li–Li interactions by accurately representing quantum mechanical potential energy curves with the Hulburt–Hirschfelder potential. It is noted that their results for metal vapour show excellent agreement with experimental results. Therefore, the excellent agreement of our calculated viscosity and thermal conductivity provides evidence that the interaction collision integrals based on the ab initio calculations can be used to accurately estimate the transport properties. In the temperature range between 4000 and 10,000 K, we can find there are large discrepancy points due to the use of different collision integrals. Holland et al. take into account the non-ionized lithium

vapour and the effects of ionization of lithium vapour are not included in their study. This leads to an overestimation of the lithium viscosity at high temperatures. Their calculated thermal conductivity is underestimated above 4000 K because the reactive thermal conductivity contributed by ionization reaction is not ignored. Our calculated values of viscosity of the lithium plasma are significantly higher than those calculated by Wang et al. [42] for temperatures from 4000 K to about 11,000 K where the neutral and charges species interaction is important. This is attributed to the different interaction potentials used. In their calculation, polarization potential is used. It has been emphasized that the estimation of the interaction energy from this classic potential can be poorly adequate and often brings about large deviation in comparison with the accurate ab initio calculation of interaction potential [18].

Similar discrepancy occurs at temperatures from 4000 K to about 11,000 K for which the reaction thermal conductivity associated with the ionization of lithium atoms is important. The charge-exchange cross-section for the Li^+–Li interaction is the main factor in determining the reactive thermal conductivity here. In Wang et al. [42] 's study, the charge-exchange cross sections of Li–Li^+ are obtained by a scaling procedure based on experimental measurements for caesium [83]. Our current work uses the transport cross section by choosing a best fit to beam measurements [68] and should be more reliable.

Above 10,000 K, the screened Coulomb potential interaction by charged species dominates in the plasma. Our calculated viscosity is higher than that by Wang et al. [42]. This is partly because of the difference in the formulations used for Debye length in the computation of Coulomb collision integrals. Wang et al. [42] includes only the contribution from electrons whereas our current work takes into account the effect of ions on the screening distance. However, it seems that the much lower values above 10,000 K by them cannot be fully explained by the different definitions of Debye Length because their value is one order lower than that obtained by the literature for single ionized plasma. In contrast, our calculated thermal conductivity shows good agreement with Wang et al. [42] 's values. The slight higher value by our work is due to the fact that the Debye length is defined by including the ions' contribution. Indeed, by using the same definition we obtain similar results.

Conclusions

Calculation of the transport coefficients under both the local thermodynamic equilibrium (LTE) and non-equilibrium (NLTE) conditions have been reported in this paper for lithium plasma extending the temperature and pressure as well as the non-equilibrium parameter currently available in literature. The accuracy of the results has been checked through comparisons with published available data. Good agreement is found in the low temperature range where neutral species interactions dominate. However, there exist discrepancies in the temperature range where ionization takes place between the present results and those available from published literature. The difference is believed to be associated with the use of different interaction potentials. For the calculation of transport coefficients, the collision integrals used here are expected to be more accurate than previously calculated values; accordingly, results presented in this paper are expected to be more accurate than those previously published.

Acknowledgements This work was supported by National Natural Science Foundation of China (Grant No. 11675040), Natural Science Foundation of Liaoning Province (Grant No. 201602175), and the Fundamental Research Funds for the Central Universities of China (Grant No. DUT15ZD (G) 01).

References

1. Kodys AD, Choueiri EY (2005) A critical review of the state-of-the-art in the performance of applied-field magnetoplasmadynamic thrusters. In: 41st AIAA/ASME/SAE/ASEE joint propulsion conference (Tucson, AZ) AIAA-2005-2447, p 1–23
2. Coogan W, Hepler MA, Choueiri E (2016) Measurement of the applied-field component of the thrust of a lithium Lorentz force accelerator. In: 52nd AIAA/ASME/SAE/ASEE joint propulsion conference AIAA propulsion and energy forum, AIAA 2016-4537
3. Xisto CM, Páscoa JC, Oliveira PJ, Nicolini DA (2012) A hybrid pressure density-based algorithm for the Euler equations at all Mach number regimes. Int J Numer Methods Fluids 70:961–976
4. Sleziona PC, Auweter-Kurtz M, Schrade HO, (1988) numerical codes for cylindrical MPD thrusters. In: Proceedings of 20th international electric propulsion conference, no. IEPC 88-038
5. Hirschfelder JO, Curtis CF, Bird RB (1964) Molecular theory of gases and liquids, 2nd edn. Wiley, New York
6. Murphy AB, Arundell CJ (1994) Transport coefficients of argon, nitrogen, oxygen, argon–nitrogen, and argon–oxygen plasmas. Plasma Chem Plasma Process 14:451–490
7. Capitelli M, Celiberto R, Gorse C, Giordano D (1995) Transport properties of high temperature air components: a review. Plasma Chem Plasma Process 16:S269–S302
8. Murphy AB (1995) Transport coefficients of air, argon–air, nitrogen–air, and oxygen–air plasmas. Plasma Chem Plasma Process 15:279–307
9. Pousse J, Chervy B, Bilodeau JF, Gleizes A (1996) Thermodynamic and transport properties of argon/carbon and helium/carbon mixtures in fullerene synthesis. Plasma Chem Plasma Process 16:605–634
10. Murphy AB (1997) Transport coefficients of helium and argon–helium plasmas. IEEE Trans Plasma Sci 25:809–814
11. Murphy AB (2000) Transport coefficients of hydrogen and argon–hydrogen plasmas. Plasma Chem Plasma Process 20:279–297
12. Cressault Y, Gleizes A (2004) Thermodynamic properties and transport coefficients in Ar–H_2–Cu plasma. J Phys D Appl Phys 37:560–572
13. Sourd B, Aubreton J, Elchinger MF, Labrot M, Michon U (2006) High temperature transport coefficients in E/C/H/N/O mixtures. J Phys D Appl Phys 39:1105–1119
14. Tanaka Y, Yamachi N, Matsumoto S, Kaneko S, Okabe S, Shibuya M (2008) Thermodynamic and transport properties of CO_2, CO_2–O_2, and CO_2–H_2 mixtures at temperatures of 300 to 30000 K and pressures of 0.1 to 10 MPa. Electr Eng Japan 163:18–29
15. Cressault Y, Hannachi R, Teulet Ph, Gleizes A, Gonnet JP, Battandier JY (2008) Influence of metallic vapours on the properties of air thermal plasmas. Plasma Sour Sci Technol 17:035016
16. Wang WZ, Murphy AB, Yan JD, Rong MZ, Spencer JW, Fang MTC (2011) Thermophysical properties of high-temperature reacting mixtures of carbon and water in the range 400–30,000 K and 0.1–10 atm: I. Equilibrium composition and thermodynamic properties. Plasma Chem Plasma Process 32:75–96
17. Wang WZ, Rong MZ, Murphy AB, Wu Y, Spencer JW, Yan JD, Fang MTC (2011) Thermophysical properties of carbon–argon and carbon–helium plasmas. J Phys D Appl Phys 44:355207
18. Wang WZ, Wu Y, Rong MZ, Éhn L, Černušák I (2012) Thermodynamic properties and transport coefficients of F_2, CF_4, C_2F_2, C_2F_4, C_2F_6, C_3F_6 and C_3F_8 plasmas. J Phys D Appl Phys 45:285201
19. Wang WZ, Yan JD, Rong MZ, Murphy AB, Spencer JW, Fang MTC (2012) Thermophysical properties of high temperature reacting mixtures of carbon and water in the range 400–30,000 K and 0.1–10 atm: II. Transport coefficients. Plasma Chem Plasma Process 32:495–518
20. Wang WZ, Wu Y, Rong MZ, Yang F (2012) Theoretical computation studies for transport properties of air plasmas. Acta Phys Sin 61:105201
21. Wang WZ, Rong MZ, Wu Y, Yan JD (2014) Fundamental properties of high-temperature SF_6 mixed with CO_2 as a replacement for SF_6 in high-voltage circuit breakers. J Phys D Appl Phys 47:255201
22. Rat V, Murphy AB, Aubreton J, Elchinger MF, Fauchais P (2008) Treatment of non-equilibrium phenomena in thermal plasma flows. J Phys D Appl Phys 41:183001
23. Girard R, Gonzalez JJ, Gleizes A (1999) Modelling of a two-temperature SF_6 arc plasma during extinction. J Phys D Appl Phys 32:1229–1238
24. Gonzalez JJ, Girard R, Gleizes A (2000) Decay and post-arc phases of a SF_6 arc plasma: a thermal and chemical non-equilibrium model. J Phys D Appl Phys 33:2759–2768
25. Trelles JP, Chazelas C, Vardelle A, Heberlein JVR (2009) Arc Plasma Torch Modeling. J Thermal Spray Technol 18:728–752
26. Colombo V, Ghedini E, Boselli M, Sanibondi P, Concetti A (2011) 3D static and time-dependent modelling of a dc transferred arc twin torch system. J Phys D Appl Phys 44:194005

27. Ghorui S, Heberlein JVR, Pfender E (2007) Non-equilibrium modelling of an oxygen-plasma cutting torch. J Phys D Appl Phys 40:1966–1976
28. Trelles JP, Heberlein JVR, Pfender E (2007) Non-equilibrium modelling of arc plasma torches. J Phys D Appl Phys 40:5937
29. Wang WZ, Yan JD, Rong MZ, Spencer JW (2013) Theoretical investigation of the decay of an SF_6 gas-blast arc using a two-temperature hydrodynamic model. J Phys D Appl Phys 46:065203
30. Wang WZ, Kong LH, Geng JY, Wei FZ, Xia GQ (2017) Wall ablation of heated compound-materials into non-equilibrium discharge plasmas. J Phys D Appl Phys 50:074005
31. Devoto RS (1967) Third approximation to the viscosity of multicomponent mixtures. Phys Fluids 10:2704–2706
32. Bonnefoi C (1983) Ph.D. thesis, Limoges University, France
33. Rat V, André P, Aubreton J, Elchinger MF, Fauchais P, Lefort A (2001) Transport properties in a two-temperature plasma: theory and application. Phys Rev E 64:26409
34. Zhang XN, Li HP, Murphy AB, Xia WD (2013) A numerical model of non-equilibrium thermal plasmas. I. Transport properties. Phys Plasmas 20:033508
35. Zhang XN, Li HP, Murphy AB, Xia WD (2015) Comparison of the transport properties of two-temperature argon plasmas calculated using different methods. Plasma Sour Sci Technol 24:035011
36. Ghorui S, Heberlein JVR, Pfender E (2008) Thermodynamic and transport properties of two-temperature nitrogen-oxygen plasma. Plasma Chem Plasma Process 28:553–582
37. Wu Y et al (2016) Calculation of 2-temperature plasma thermos-physical properties considering condensed phases: application to CO_2–CH_4 plasma: part 1. Composition and thermodynamic properties. J Phys D Appl Phys 49:405203
38. Miller EM, Sandler SI (1973) Transport properties of two-temperature partially ionized argon. Phys Fluids 16:491–493
39. Kannappan D, Bose TK (1977) Transport properties of a two-temperature argon plasma. Phys Fluids 20:1668–1673
40. Rat V, Andre P, Aubreton J (2002) Transport coefficients including diffusion in a two-temperature argon plasma. J Phys D Appl Phys 35:981–991
41. Kannappan DB, Bose TK (1980) Transport properties of a two-temperature helium plasma. Phys Fluids 23:1473–1474
42. Wang HY et al (2017) Thermodynamic properties and transport coefficients of two temperature PTFE vapour plasma for ablation controlled discharge applications. J Phys D Appl Phys. doi:10.1088/1361-6463/aa7d68
43. Wang HX, Sun SR, Chen SQ (2012) Calculation of two-temperature transport coefficients of helium plasma. Acta Phys Sin 61:195203
44. Rat V, Andre P, Aubreton J, Elchinger MF, Fauchais P, Lefort A (2002) Two-temperature transport coefficients in argon–hydrogen plasmas: I. Elastic processes and collision integrals. Plasma Chem Plasma Process 22:453–474
45. Niu CP et al (2016) Calculation of 2-temperature plasma thermo-physical properties considering condensed phases: application to CO_2–CH_4 plasma: part 2. Transport coefficients. J Phys D Appl Phys 49:405204
46. Wang WZ, Rong MZ, Wu Y, Spencer JW, Yan JD, Mei DH (2012) Thermodynamic and transport properties of two-temperature SF_6 plasmas. Phys Plasmas 19:3–18
47. Wang WZ, Rong MZ, Yan JD, Murphy AB, Spencer JW (2011) Thermophysical properties of nitrogen plasmas under thermal equilibrium and non-equilibrium conditions. Phys Plasmas 18:113502
48. Aubreton J, Elchinger MF, Rat V (2004) Two-temperature transport coefficients in argon–helium thermal plasmas. J Phys D Appl Phys 37:34–41
49. Colombo V, Ghedini E, Sanibondi P (2009) Two-temperature thermodynamic and transport properties of argon–hydrogen and nitrogen–hydrogen plasmas. J Phys D Appl Phys 42:055213
50. Colombo V, Ghedini E, Sanibondi P (2011) Two-temperature thermodynamic and transport properties of carbon–oxygen plasmas. Plasma Sour Sci Technol 20:03500
51. Wang HX, Chen SQ, Chen X (2012) Thermodynamic and transport properties of two-temperature lithium plasmas. J Phys D Appl Phys 45:165202
52. Murphy AB (2001) Thermal plasmas in gas mixtures. J Phys D Appl Phys 34:151–173
53. Potapov AV (1966) Chemical equilibrium of multi-temperature systems. High Temp 4:48–51
54. van de Sanden MCM, Schram PPJM, Peeters AG, van der Mullen JAM, Kroesen GMW (1989) Thermodynamic generalization of the Saha equation for a two-temperature plasma. Phys Rev A 40:5273–5276
55. Giordano D (1998) Equivalence of energy, entropy, and thermodynamic potentials in relation to the thermodynamic equilibrium of multitemperature gas mixtures. Phys Rev E 58:3098–3112

56. Giordano D, Capitelli M (2001) Nonuniqueness of the two-temperature Saha equation and related considerations. Phys Rev E 65:16401
57. White WB, Johnson SM, Dantzig GB (1958) Chemical equilibrium in complex mixtures. J Chem Phys 28:751
58. Andre P (1995) Partition functions and concentrations in plasmas out of thermal equilibrium. IEEE Trans Plasma Sci 23:453–458
59. Andre P, Abbaoui M, Lefort A, Parizet MJ (1996) Numerical method and composition in multi-temperature plasmas: application to an Ar-H_2 mixture. Plasma Chem Plasma Process 16:379–398
60. Chen X, Han P (1999) On the thermodynamic derivation of the Saha equation modified to a two-temperature plasma. J Phys D Appl Phys 32:1711–1718
61. Giordano D, Capitelli M (1995) Two-temperature Saha equation—a misunderstood problem. J Thermophys Heat Transfer 9:803–804
62. Andre P, Aubreton J, Elchinger MF, Rat V, Fauchais P, Lefort A, Murphy AB (2004) A statistical mechanical view of the determination of the composition of multi-temperature plasmas. Plasma Chem Plasma Process 24:435–446
63. Wang WZ, Rong MZ, Spencer JW (2013) Nonuniqueness of two-temperature Guldberg–Waage and Saha equations: influence on thermophysical properties of SF_6 plasmas. Phys Plasmas 20:113504
64. Ralchenko Y, Kramida AE, Reader J, NIST ASD Team 2008 NIST atomic spectra database (version 3.1.5). National Institute of Standards and Technology, Gaithersburg, MD http://physics.nist.gov/PhysRefData/ASD/levels_form.html
65. Zavitsas AA (2003) The potential energy curve of the ground state of lithium $X^1\Sigma_g^+$ Li_2. J Mol Spectrosc 221:67–71
66. Kutzelnigg W, Staemmler V, Oelus M (1972) Potential curve of the lowest triplet state of Li_2. Chem Phys Lett 13:496–500
67. Jasika P, Wilczyński J, Sienkiewicz JE (2007) Calculation of adiabatic potentials of Li_2^+. Eur Phys J Special Topics 144:85–91
68. Lorents DC, Black G, Heinz O (1965) Charge transfer between Li ions and Li atoms in the 14-1000-eV energy region. Phys Rev A 137:1049
69. Li TC, Liu CH, Qu YC et al (2015) Resonant charge transfer in slow Li^+–Li(2s) collisions. Chin Phys B 24:103401
70. Johnson WR, Safronova UI, Derevianko A, Safronova MS (2008) Relativistic many-body calculation of energies, lifetimes, hyperfine constants, and polarizabilities in ^{7}Li. Phys Rev A 77:022510
71. Bray I (1998) Private Communication
72. Williams W, Trajmar S, Bozinis D (1976) Electron scattering from Li at 5.4, 10, 20 and 60 eV impact energies. J Phys B At Mol Phys 9:1529–1536
73. Mason EA, Munn RJ (1967) Transport coefficients of ionized gases. Phys Fluids 10:1827–1832
74. Devoto RS (1973) Transport properties of ionized gases. Phys Fluids 16:616–623
75. Ghorui S, Das AK (2013) Collision integrals for charged-charged interaction in two-temperature non-equilibrium plasma. Phys Plasmas 20:093504
76. Chapman S, Cowling TG (1970) The mathematical theory of non-uniform gases, 3rd edn. Cambridge University Press, Cambridge
77. Ferziger JH, Kaper HG (1972) Mathematical theory of transport processes in gases. North-Holland, Amsterdam
78. Wang WZ, Rong MZ, Yan JD, Wu Y (2002) The reactive thermal conductivity of thermal equilibrium and nonequilibrium plasmas: application to nitrogen. IEEE Trans Plasma Sci 40:980–989
79. Xi Chen, Li HP (2003) The reactive thermal conductivity for a two-temperature plasma. Int J Heat Mass Transfer 46:1443–1454
80. Boulos MI, Fauchais P, Pfender E (1994) Thermal plasmas: fundamentals and applications. Plenum, New York
81. Holland PM, Biolsi L, Rainwater JC (1986) Theoretical calculation of the transport properties of monatomic lithium vapor. J Chem Phys 85:4011–4018
82. Gleizes A, Chervy B, Gonzalez JJ (1999) Calculation of a two-temperature plasma composition: bases and application to SF_6. J Phys D Appl Phys 32:2060–2067
83. Davies RH, Mason EA, Munn RJ (1965) High-temperature transport properties of alkali metal vapors. Phys Fluids 8:444–452